

Mixed Convection in a Ventilated Cavity Filled with a Triangular Porous Layer

Nikita S. Gibanov¹ · Mikhail A. Sheremet^{1,2} ·
Muneer A. Ismael³ · Ali J. Chamkha^{4,5}

Received: 4 March 2017 / Accepted: 20 June 2017 / Published online: 11 September 2017
© Springer Science+Business Media B.V. 2017

Abstract Mixed convection in a square cavity having a triangular porous layer and a local heater has been investigated numerically. The governing partial differential equations with corresponding boundary conditions have been solved by the finite difference method using the dimensionless stream function, vorticity and temperature formulation. The effects of the Richardson number ($Ri = 0.01 - 10$), Darcy number ($Da = 10^{-7} - 10^{-1}$), heater length ($\delta = H/L = 0.2 - 0.4$) and different locations of the porous layer on the streamlines and isotherms as well as the average and local Nusselt numbers at the heater have been analyzed. It has been found that all these key parameters essentially affect the flow and heat transfer patterns.

Keywords Mixed convection · Square ventilated cavity · Porous layer · Numerical results

List of symbols

A	Thermal diffusivity ratio ($A = \alpha_{\text{eff}}/\alpha_f$)
c_p	Specific heat at constant pressure ($\text{J kg}^{-1}\text{K}^{-1}$)
Da	Darcy number ($Da = K/L^2$)
g	Gravitational field (m s^{-2})

✉ Muneer A. Ismael
muneer.ismael.ecb@uobasrah.edu.iq; muneerismael@yahoo.com

¹ Laboratory on Convective Heat and Mass Transfer, Tomsk State University, Tomsk, Russia 634050

² Department of Nuclear and Thermal Power Plants, Tomsk Polytechnic University, Tomsk, Russia 634050

³ Mechanical Engineering Department, Engineering College, University of Basrah, Basrah, Iraq

⁴ Mechanical Engineering Department, Prince Mohammad Bin Fahd University, Al-Khobar 31952, Saudi Arabia

⁵ Prince Sultan Endowment for Energy and Environment, Prince Mohammad Bin Fahd University, Al-Khobar 31952, Saudi Arabia

Gr	Grashof number ($Gr = \frac{g \beta_f (T_h - T_c) L^3}{\nu_f^2}$)
H	Heating element length (m)
K	Permeability of porous medium (m^2)
k	Thermal conductivity ($W m^{-1} K^{-1}$)
L	Cavity length (m)
n	Normal vector
Nu	Local Nusselt number
\overline{Nu}	Average Nusselt number
p	Pressure (Nm^{-2})
Pr	Prandtl number ($Pr = \nu_f / \alpha_f$)
Re	Reynolds number ($Re = u_{in} L / \nu_f$)
Ri	Richardson number ($Ri = Gr / Re^2$)
S, S_1, S_2	Side lengths of the triangular porous layer (m)
T	Temperature (K)
U	Dimensionless velocity component along x -direction
u	Velocity component along x -direction ($m s^{-1}$)
u_{in}	Inlet velocity ($m s^{-1}$)
V	Dimensionless velocity component along y -direction
v	Velocity component along y -direction ($m s^{-1}$)
X, Y	Dimensionless Cartesian coordinates
x, y	Cartesian coordinates (m)

Greek symbols

α	Thermal diffusivity ($m^2 s^{-1}$)
β	Thermal expansion coefficient (K^{-1})
δ	Dimensionless length of heating element ($\delta = H/L$)
ε	Porosity of the porous layer
μ	Dynamic viscosity (Pa s)
ν	Kinematic viscosity ($m^2 s^{-1}$)
θ	Dimensionless temperature
Λ	Thermal conductivity ratio ($\Lambda = k_{eff} / k_f$)
ρ	Density ($kg m^{-3}$)
ψ	Stream function ($m^2 s^{-1}$)
Ψ	Dimensionless stream function
ω	Vorticity (s^{-1})
Ω	Dimensionless vorticity

Subscripts

c	Cold
eff	Effective
f	Fluid
h	Hot
p	Porous
s	Solid matrix forming the porous medium

1 Introduction

Mixed convection inside enclosure is still one of the researcher's interested vehicles because it is a useful tool of heat transfer augmentation. It provides efficient cooling (or heating) for many engineering applications like building ventilation, cooling of electronic devices, cooling of chemical reactors and emergency cooling system of nuclear reactors. Several studies have confirmed different issues of mixed convection according to the geometry of the flow channel. For ventilation requirements and optimal performance, the flow channel can be designed in various different shapes. [Mezrhab et al. \(2010\)](#) have considered a vented T-shaped cavity. [Biserni et al. \(2007\)](#) optimized the geometry of H-shaped cavity. [Pardeshi \(2013\)](#) investigated the L-shaped cooling passage for the trailing edge of gas turbine blade with a combination of ribs and pin fins.

A growing interest of reinforcing the natural convection in square or rectangular enclosures has led to extensive studies and innovations; one of these is providing the enclosed cavities by vents, i.e., switching the forced convection, which its interaction with the natural convection can augment the heat transfer process. [Angirasa \(2000\)](#) has discussed the complex interaction between the natural and forced convection in square vented cavity, where the inlet and vent ports were situated at the left edges of the bottom and top walls, respectively. He declared to an augmented heat transfer when Reynolds number increased. [Boulard et al. \(2002\)](#) have reviewed and simulated the turbulent convection in the ventilated greenhouse, which are provided by heating pipes. They discussed the improvement of the greenhouse climate through better plant protection and enhancements of the design and control aspects of the greenhouse. [Raji et al. \(2008\)](#) have discussed the mixed convection in a rectangular cavity supplied by air jet from an inlet at the left vertical wall, and the flow exits from a vent at the opposing wall. They constructed relations for heat transfer by forced convection and confirmed the interaction between natural and forced convective modes. There are special applications like cables of electric transmission, fire research, and brake housing of an aircraft ([Desai and Vafai 1992](#)) which can be modeled as an open-ended cavities. Studies interested in this practical topic are carried out experimentally ([Chen et al. 1985](#); [Showole and Tarasuk 1993](#); [Elsayed and Chakroun 1999](#)) and analytically ([Vafai and Etefagh 1990a, b](#); [Mhiri et al. 1998](#); [Besbes et al. 2001](#); [Khanafer and Vafai 2000, 2002](#); [Khanafer et al. 2002](#)). Two distinct conclusions can be drawn from these studies. The first is that the heat transfer coefficient has no clear relation with the tilting angle and the configuration of the cavity, and the second is that when the flow is normal to the open-ended side this will act as an insulator between the cavity and the surrounding medium ([Khanafer and Vafai 2002](#)). [Anil Lal and Reji \(2009\)](#) have employed the restricted domain approach to study the natural convection in an open-edge cavity with vented sidewalls. They reviewed various numerical techniques implemented in simulation of natural convection in open cavity. [Xu et al. \(2014\)](#) conducted a numerical study regarding the double-diffusive mixed convection in a square vented enclosure containing a circular cylinder of high temperature and concentration fixed at the middle of the cavity. They predicted complicated interactions between the mixed convection parameter (Richardson number) and the double-diffusive parameters (Lewis number and buoyancy ratio). [Kuznetsov and Sheremet \(2010\)](#) have analyzed numerically conjugate mixed convection in a ventilated cavity with a local heater. They obtained the diagram of the heat convection modes depending on the Grashof and Reynolds numbers. [Ghalambaz et al. \(2017\)](#) have studied triple-diffusive mixed convective heat and mass transfer of a mixture in an enclosure filled with a Darcy porous medium. The results indicated that the presence of one pollutant phase could significantly affect the pollutant distribution of the other phase.

However, when the heat transfer augmentation is a challenging issue, the mixed convection can be supported by improving the properties of the working fluid. Over the past decade, nanofluid was demonstrated as a powerful interesting field in heat transfer enhancement. It is the dispersing of nanosized solid particles of superior thermal conductivity into the working base fluid (Choi and Eastman 1995). The resulting mixture experiences an improved thermal conductivity and increased heat capacity. Nanofluid is familiar strategy in enclosures (Tiwari and Das 2007); nevertheless, they are also used in vented cavities; Mahmoudi et al. (2010), Shahi et al. (2010), Nasrin et al. (2013), Bahlaoui et al. (2016) and Sheremet et al. (2015). It is worth mentioning that in practice, these vented cavities are parts of enclosed loop system because the nanofluid is toxic and expensive; thus, it is not acceptable to discharge it to environment. The common feature among these studies (except in some situations) is that the heat transfer increases with increasing the volume fraction of the nanoparticles.

Porous media are encountered in many industrial and environmental situations surrounding us such as solar collectors and food applications. Plenty variety of studies regarding the convection in saturated porous enclosures along with their respective applications are described in very interested books of Nield and Bejan (2017), Ingham and Pop (2005), Vafai (2015) and Shenoy et al. (2016). A first published study debating the effect of ventilating enclosures saturated with porous media may be referred to Mahmud and Pop (2006). They adopted the geometry of Angirasa (2000), but for porous medium with relatively low modified Rayleigh number ($Ra \leq 1000$), i.e., they assumed the Darcy model. They coded the problem using finite volume method and based the geometry representation on the finite element approach. They found that the flow and heat transfer are significantly sensitive to the width of the inlet and vent ports. Behzadi et al. (2015) investigated the mixed convection in a square enclosure filled with porous media provided with inlet, at the lower of the left wall, and vent at the upper of the right wall. They used Darcy–Brinkman model to simulate the fluid flow within the porous medium. They showed that when the Darcy number and the diameter of the particles forming the porous matrix increase, the mean heat transfer decreases.

In practice, there are many applications requiring coupling the momentum exchange between two adjacent layers: porous layer and homogeneous fluid layer. Filtration processes, drying process, material solidification, pollution of ground water and many other biological applications are some of the practical issues of such geometry. Different configurations of superimposed adjacent two layers, confined in enclosures have been extensively studied by Beavers and Joseph (1967), Kim et al. (1987), Chen and Chen (1992), Kim and Choi (1996), Zhao and Chen (2001), Lopez and Tapia (2001), Hirata et al. (2009), Bagchi and Kulacki (2012), Sheremet and Trifonova (2013), Sheremet and Trifonova (2013), Beckermann et al. (1987), Gobin et al. (2005), Chamkha and Ismael (2014), Ismael and Chamkha (2015) and Arpino et al. (2015). The common finding of these studies is that the existence of the porous layer in a specified thickness and porosity can significantly affect the behavior of the flow and heat.

However, the literature review above led us to be certain and to the best of the authors' knowledge that the problem of mixed convection in a vented square cavity with a triangular porous layer has not been examined yet. Hence, the numerical solution and investigation will be the objective of the current study. It is believed that this study will reveal the contributions of enhancing the thermal performance in porous cavities, which has industrial applications significance particularly in solar collectors with a porous absorber, grain storage/drying and modeling with an interested inclined interface.

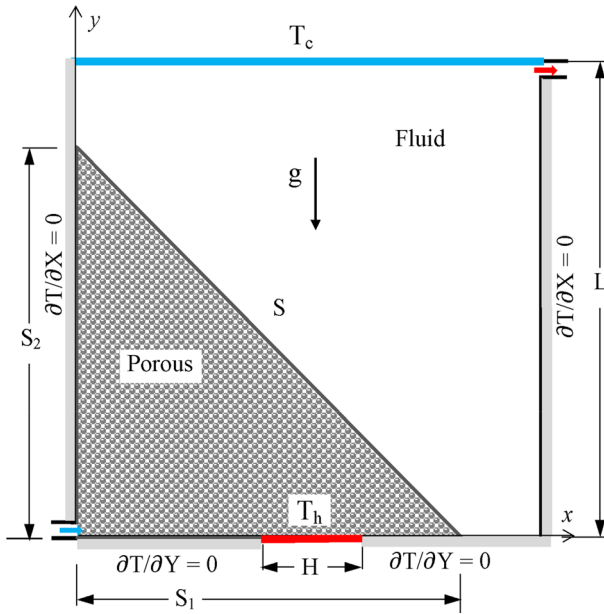


Fig. 1 Schematic of the present problem

2 Problem Definition

The present study concerns with mixed convection in a composite square cavity with side length of L as shown in Fig. 1. The cavity is composed of two layers such as a triangular porous layer confined with a fluid (water or air). The porous layer is saturated with the same fluid. An input and output ports are localized at the lower and upper ends of the left and right walls, respectively, with an opening value of say $L/10$. The left and right walls of the cavity are thermally insulated. A hot element is localized at the bottom wall with $T = T_h$ and size of $H = L/4$. The top wall is kept isothermal at cold temperature T_c . Cavity walls are impermeable except the inclined interface between the porous layer and the fluid. The Brinkman–extended Darcy model is invoked for the momentum exchange within the porous layer.

The Navier–Stokes equations based on the previous assumptions in Cartesian coordinates for (porous and fluid layers) can be written as follows:

For the porous layer:

Continuity equation:

$$\frac{\partial u_p}{\partial x} + \frac{\partial v_p}{\partial y} = 0 \tag{1}$$

x -direction momentum equation:

$$\rho_f \left(u_p \frac{\partial u_p}{\partial x} + v_p \frac{\partial u_p}{\partial y} \right) = -\varepsilon^2 \frac{\partial p}{\partial x} + \varepsilon \mu_f \left(\frac{\partial^2 u_p}{\partial x^2} + \frac{\partial^2 u_p}{\partial y^2} \right) - \varepsilon^2 \frac{\mu_f}{K} u_p \tag{2}$$

y-direction momentum equation:

$$\rho_f \left(u_p \frac{\partial v_p}{\partial x} + v_p \frac{\partial v_p}{\partial y} \right) = -\varepsilon^2 \frac{\partial p}{\partial y} + \varepsilon \mu_f \left(\frac{\partial^2 v_p}{\partial x^2} + \frac{\partial^2 v_p}{\partial y^2} \right) - \varepsilon^2 \frac{\mu_f}{K} v_p + \varepsilon^2 \rho_f \beta_f g (T_p - T_c) \quad (3)$$

Energy equation:

$$u_p \frac{\partial T_p}{\partial x} + v_p \frac{\partial T_p}{\partial y} = \alpha_{\text{eff}} \left(\frac{\partial^2 T_p}{\partial x^2} + \frac{\partial^2 T_p}{\partial y^2} \right) \quad (4)$$

For the fluid layer:

Continuity equation:

$$\frac{\partial u_f}{\partial x} + \frac{\partial v_f}{\partial y} = 0 \quad (5)$$

x-direction momentum equation:

$$\rho_f \left(u_f \frac{\partial u_f}{\partial x} + v_f \frac{\partial u_f}{\partial y} \right) = -\frac{\partial p}{\partial x} + \mu_f \left(\frac{\partial^2 u_f}{\partial x^2} + \frac{\partial^2 u_f}{\partial y^2} \right) \quad (6)$$

y-direction momentum equation:

$$\rho_f \left(u_f \frac{\partial v_f}{\partial x} + v_f \frac{\partial v_f}{\partial y} \right) = -\frac{\partial p}{\partial y} + \mu_f \left(\frac{\partial^2 v_f}{\partial x^2} + \frac{\partial^2 v_f}{\partial y^2} \right) + \rho_f \beta_f g (T_f - T_c) \quad (7)$$

Energy equation:

$$u_f \frac{\partial T_f}{\partial x} + v_f \frac{\partial T_f}{\partial y} = \alpha_f \left(\frac{\partial^2 T_f}{\partial x^2} + \frac{\partial^2 T_f}{\partial y^2} \right) \quad (8)$$

For the given problem, the appropriate boundary conditions at the system boundaries are:

1. at $y = 0$ (bottom wall) and $\frac{L-H}{2} \leq x \leq \frac{L+H}{2}$ we have $T = T_h$, otherwise, $\frac{\partial T}{\partial y} = 0$
2. at $y = H$ (top wall) $T = T_c$
3. at $x = 0$ (left wall) and $x = L$ (right wall) $\frac{\partial T}{\partial x} = 0$
4. in the input vent: $u = u_{\text{in}}$, $v = 0$, and in the outlet vent, $p = 0$ and $v = 0$
5. along the interface line S :

Continuity of horizontal and vertical velocity components, $u_p = u_f$, $v_p = v_f$

Shear stress, Neale and Nader (1974), $\mu_{\text{eff}} \left(\frac{\partial u}{\partial y} + \frac{\partial v}{\partial x} \right)_p = \mu_f \left(\frac{\partial u}{\partial y} + \frac{\partial v}{\partial x} \right)_f$

Continuity of pressure, $p_p = p_f$

Temperature and heat flux, $T_p = T_f$, $-k_{\text{eff}} \frac{\partial T_p}{\partial n} = -k_f \frac{\partial T_f}{\partial n}$.

The formulation is based on the stream function, $u = \frac{\partial \psi}{\partial y}$, $v = -\frac{\partial \psi}{\partial x}$ and the vorticity, $\omega = \frac{\partial v}{\partial x} - \frac{\partial u}{\partial y}$, and on the following non-dimensional parameters:

$$X = \frac{x}{L}, \quad Y = \frac{y}{L}, \quad U = \frac{u}{u_{\text{in}}}, \quad V = \frac{v}{u_{\text{in}}}, \quad P = \frac{(p + \rho_f g y)}{\rho_f u_{\text{in}}^2},$$

$$\Psi = \frac{\psi}{u_{\text{in}} L}, \quad \Omega = \frac{\omega L}{u_{\text{in}}}, \quad \theta = \frac{T - T_c}{T_h - T_c}$$

Following the usual manipulation of eliminating pressure gradient terms from momentum equations, the dimensionless governing equations become:

For porous layer:

$$\frac{\partial^2 \Psi_p}{\partial X^2} + \frac{\partial^2 \Psi_p}{\partial Y^2} = -\Omega_p \tag{9}$$

$$\frac{\partial \Psi_p}{\partial Y} \frac{\partial \Omega_p}{\partial X} - \frac{\partial \Psi_p}{\partial X} \frac{\partial \Omega_p}{\partial Y} = \frac{\varepsilon}{Re} \left(\frac{\partial^2 \Omega_p}{\partial X^2} + \frac{\partial^2 \Omega_p}{\partial Y^2} - \frac{\varepsilon}{Da} \Omega_p \right) + \varepsilon^2 Ri \frac{\partial \theta_p}{\partial X} \tag{10}$$

$$\frac{\partial \Psi_p}{\partial Y} \frac{\partial \theta_p}{\partial X} - \frac{\partial \Psi_p}{\partial X} \frac{\partial \theta_p}{\partial Y} = \frac{\alpha_{eff}/\alpha_f}{Re \cdot Pr} \left(\frac{\partial^2 \theta_p}{\partial X^2} + \frac{\partial^2 \theta_p}{\partial Y^2} \right) \tag{11}$$

and for clear fluid:

$$\frac{\partial^2 \Psi_f}{\partial X^2} + \frac{\partial^2 \Psi_f}{\partial Y^2} = -\Omega_f \tag{12}$$

$$\frac{\partial \Psi_f}{\partial Y} \frac{\partial \Omega_f}{\partial X} - \frac{\partial \Psi_f}{\partial X} \frac{\partial \Omega_f}{\partial Y} = \frac{1}{Re} \left(\frac{\partial^2 \Omega_f}{\partial X^2} + \frac{\partial^2 \Omega_f}{\partial Y^2} \right) + Ri \frac{\partial \theta_f}{\partial X} \tag{13}$$

$$\frac{\partial \Psi_f}{\partial Y} \frac{\partial \theta_f}{\partial X} - \frac{\partial \Psi_f}{\partial X} \frac{\partial \theta_f}{\partial Y} = \frac{1}{Re \cdot Pr} \left(\frac{\partial^2 \theta_f}{\partial X^2} + \frac{\partial^2 \theta_f}{\partial Y^2} \right) \tag{14}$$

The appropriate dimensionless boundary conditions can be written in following form:

1. at $Y = 0 (\Omega = -\frac{\partial^2 \Psi}{\partial Y^2}, \Psi = 0)$ and $\frac{1-H/L}{2} \leq X \leq \frac{1+H/L}{2}, \theta = 1$, otherwise, $\frac{\partial \theta}{\partial Y} = 0$.
2. at $Y = 1 (\Omega = -\frac{\partial^2 \Psi}{\partial Y^2}, \Psi = 0)$ and $\theta = 0$.
3. at $X = 0$ (left wall) and $X = 1$ (right wall) $\frac{\partial \theta}{\partial X} = 0, \Omega = -\frac{\partial^2 \Psi}{\partial X^2}, \Psi = 0$
4. in the input port $\Omega = 0, \frac{\partial \Psi}{\partial Y} = 1$, and in the output port $\frac{\partial \theta}{\partial X} = \frac{\partial \Psi}{\partial X} = \frac{\partial \Omega}{\partial X} = 0$
5. The interface boundary conditions are derived from equating (continuity) of tangential and normal velocities, temperature and the heat flux across the interface. Hence, the interface conditions can be written as follows:

$$\theta_p = \theta_f, \frac{\partial \theta_f}{\partial n} = \frac{k_{eff}}{k_f} \frac{\partial \theta_p}{\partial n} \tag{15a}$$

$$\Psi_p = \Psi_f, \frac{\partial \Psi_f}{\partial n} = \frac{\partial \Psi_p}{\partial n} \tag{15b}$$

$$\Omega_p = \Omega_f, \frac{\partial \Omega_f}{\partial n} = \frac{\partial \Omega_p}{\partial n} \tag{15c}$$

Here Eqs. (15b) and (15c) were derived from the continuity of horizontal and vertical velocity components.

The following relation can calculate the effective thermal conductivity of porous medium

$$k_{eff} = (1 - \varepsilon) k_s + \varepsilon k_f \tag{16}$$

The dynamic viscosity in both layers is assumed equal ($\mu_{eff} = \mu_f$). The agreement of this assumption was proved experimentally by [Neale and Nader \(1974\)](#) and adopted by [Sheremet and Trifonova \(2013\)](#) and [Sheremet and Trifonova \(2014\)](#).

The local Nusselt number along the heater is $Nu = -\frac{\partial \theta}{\partial Y}$.

The average Nusselt number at the heater is defined as follows:

$$Nu_{avg} = \frac{L}{H} \int_{0.5(1-H/L)}^{0.5(1+H/L)} Nu \, dX \tag{17}$$

Table 1 Comparison of the average Nusselt number at the hot wall

Da	Ra	Lauriat and Prasad (1989)	Bhardwaj et al. (2015)	Present results
10^{-4}	10^5	1.06	1.08	1.07
	10^6	2.84	2.95	2.87
10^{-2}	10^3	1.02	1.02	1.02
	10^4	1.70	1.73	1.71
	10^5	4.26	4.30	4.18
	5×10^5	7.10	7.31	7.07

3 Numerical Method

The partial differential equations (9)–(14) with the corresponding boundary conditions have been solved by the finite difference method. Detailed description of the used numerical technique has been presented earlier in Kuznetsov and Sheremet (2010), Sheremet et al. (2015), Shenoy et al. (2016), Sheremet and Trifonova (2013) and Sheremet and Trifonova (2014).

The present model, in the form of an in-house computational fluid dynamics code, has been validated successfully against the works of Lauriat and Prasad (1989) and Bhardwaj et al. (2015) for natural convection in a non-Darcian porous cavity. The results presented in Table 1 show a good comparison for the average Nusselt number at the hot wall between the obtained data and the numerical data of other authors.

In the case of natural convection in a composite cavity, the benchmark solution has been obtained by using the results of Singh and Thorpe (1995). The laminar natural convection in a cavity containing a fluid layer overlying a porous layer saturated with the same fluid is analyzed. The enclosure is heated on one vertical wall and cooled on the opposite wall, while the top and bottom walls are adiabatic. Figures 2 and 3 show a good agreement between the obtained streamlines and isotherms at different Rayleigh numbers and the results by Singh and Thorpe (1995) for the case when the height of the porous layer is equal to the height of the fluid layer. Results on the basis of the Brinkman–extended Darcy model is (—) and on the basis of the Darcy model is (- - -).

We have conducted also the grid independent test, analyzing natural convection in the considered cavity presented in Fig. 1 for $Ri = 1$, $Da = 10^{-3}$, $Pr = 6.26$, $Re = 100$, $\varepsilon = 0.398$, $\Lambda = A = 1.2042$, $\delta = H/L = 0.3$, $S_1 = S_2 = 0.75L$. Five cases of the uniform grid are tested: a grid of 60×60 points, a grid of 100×100 points, a grid of 200×200 points, a grid of 300×300 points and a grid of 400×400 points. Table 2 shows the effect of the mesh parameters on the average Nusselt number of the heater.

Taking into account the conducted verifications, the uniform grid of 200×200 points has been selected for the further investigation.

4 Results and Discussion

The considered problem has been analyzed at the following values of the governing parameters: Richardson number ($Ri = 0.01 - 10$), Darcy number ($Da = 10^{-7} - 10^{-1}$),

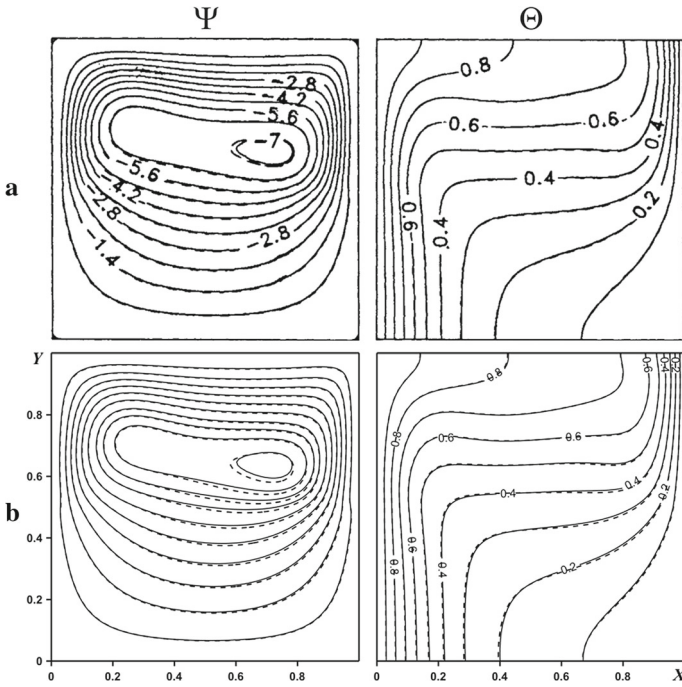


Fig. 2 Comparison of streamlines Ψ and isotherms Θ at $Da = 10^{-5}$, $Ra = 10^5$: numerical results of Singh and Thorpe (1995) (a), present study (b)

Prandtl number ($Pr = 6.26$), Reynolds number ($Re = 100$), thermal conductivity ratio ($A = k_{eff}/k_f = 1.2042$), thermal diffusivity ratio ($A = \alpha_{eff}/\alpha_f = 1.2042$), porosity ($\varepsilon = 0.398$), heat source length ($\delta = H/L = 0.2 - 0.4$) and the following geometry of the triangular porous layer: (I) $S_1 = S_2 = 0.75L$, (II) $S_1 = L$, $S_2 = 0.5L$ and (III) $S_1 = 0.5L$, $S_2 = L$. Particular efforts have been focused on the effects of these parameters on the fluid flow and heat transfer inside the cavity. Streamlines and isotherms as well as the average Nusselt number for different values of key parameters mentioned above are illustrated in Figs. 4, 5, 6, 7, 8, 9, 10, 11, 12, 13, 14, 15, 16, 17, 18 and 19.

Figure 4 presents distributions of the streamlines and isotherms for case (I) at $Da = 10^{-3}$, $\delta = 0.3$ and different values of the Richardson number. The line in the streamlines and isotherms reflects a location of a porous layer as presented in Fig. 1. Low Richardson numbers ($Ri \leq 1.0$) for the case (I) characterize a formation of a flow from the inlet to the outlet without significant circulations. Only one minor recirculation appears near the inlet due to the effect of the porous layer. At the same time, one can find a formation of a small vortex in the right bottom corner. This vortex vanishes with a growth of the Richardson number. High values of Ri illustrate an appearance of additional recirculation in the upper part of the cavity. It should be noted that a rise of the Richardson number is due to a growth of the Grashof number. The Grashof number in the present problem reflects the temperature differences between the bottom heater and the top cooler. Therefore, high values of Gr characterize an essential vertical temperature difference that leads to a formation of a convective cell inside the cavity while the main flow is distorted close to the bottom and right walls. The temperature field supplements the whole thermohydrodynamic behavior. The thermal plume formed over the heater develops along the right adiabatic wall because the incoming fluid is cold which

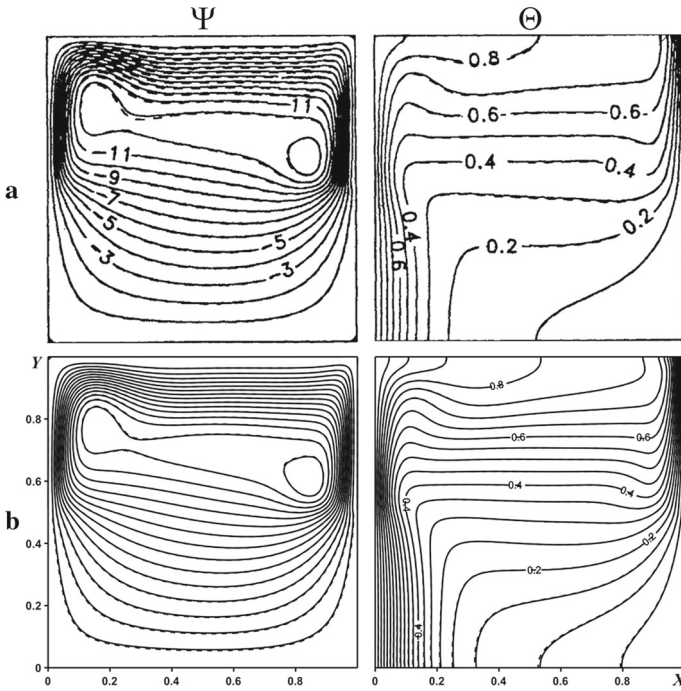


Fig. 3 Comparison of streamlines Ψ and isotherms Θ at $Da = 10^{-5}$, $Ra = 10^6$: numerical results of Singh and Thorpe (1995) (a), present study (b)

Table 2 Variations of the average Nusselt number of the heater with the uniform grids

Uniform grids	\overline{Nu}	$\Delta = \frac{ \overline{Nu}_{i \times j} - \overline{Nu}_{200 \times 200} }{\overline{Nu}_{i \times j}} \times 100\%$
60×60	12.2002	1.88
100×100	12.2662	1.34
200×200	12.43	–
300×300	12.4544	0.2
400×400	12.5335	0.83

deforms this thermal plume. Also, one can find that an increase in the Richardson number leads to a reduction of the thermal boundary layer thickness along the right vertical wall due to the effect of the incoming cold flow.

Figure 5 shows profiles of the horizontal velocity and temperature at the middle cross section $x = 0.5$. As has been mentioned above, an increase in Ri leads to an augmentation of the velocity along the bottom wall while in the upper part, the horizontal velocity decreases and for $Ri = 10.0$ one can find a formation of reverse flow. It is worth noting that a border of the porous layer in the velocity profiles is inconspicuous due to the high value of the Darcy number. The temperature profiles at $x = 0.5$ also illustrate a significant decrease in temperature along a small distance. One can observe that the dimensionless temperature reduces from 1.0 at the heater to 0.0 at 30% of the cavity height and this magnitude decreases with Ri .

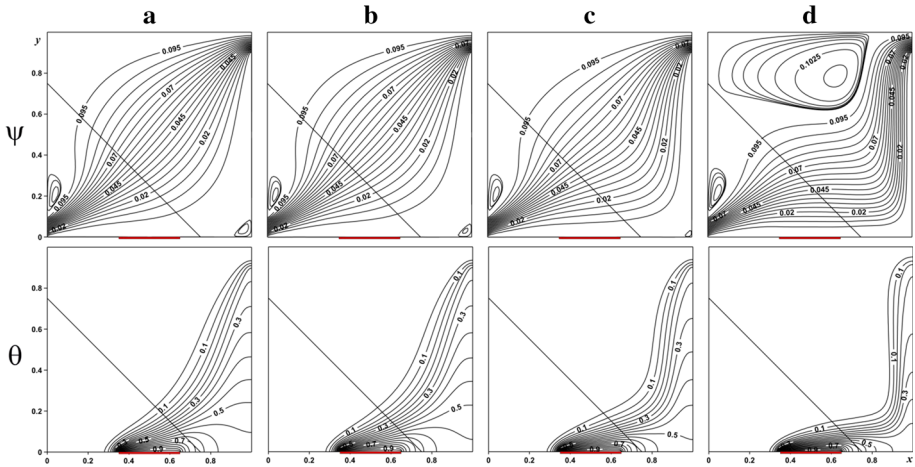


Fig. 4 Streamlines ψ and isotherms θ for case (I) at $Da = 10^{-3}$, $\delta = 0.3$: $Ri = 0.01$ (a), $Ri = 0.1$ (b), $Ri = 1.0$ (c), $Ri = 10.0$ (d)

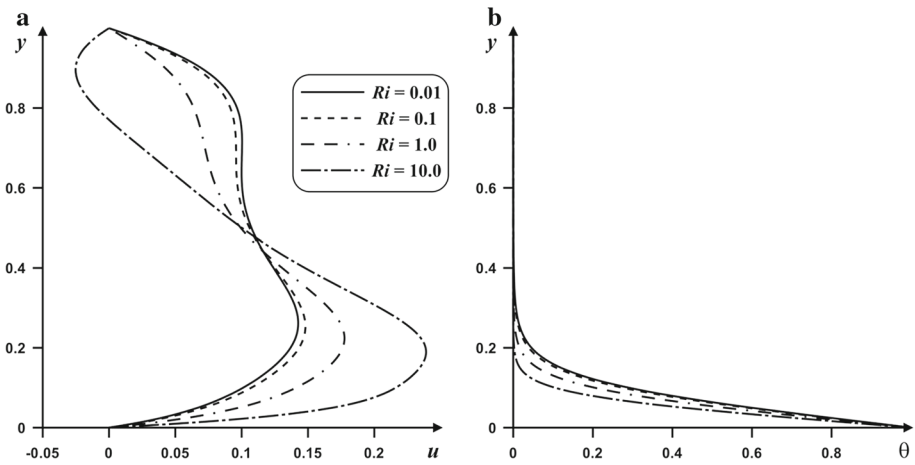


Fig. 5 Profiles of horizontal velocity u (a) and temperature θ (b) at middle cross section $x = 0.5$ for case (I) at $Da = 10^{-3}$, $\delta = 0.3$ and different Richardson numbers

In the case of the vertical velocity and temperature profiles along the horizontal cross section $y = 0.5$ (Fig. 6), it is possible to note an essential flow acceleration near the right adiabatic wall with an increase in the Richardson number, while the fluid flow in the left part of the cavity is attenuated. A growth of Ri leads to the temperature reduction close to the right vertical wall.

Figure 7 presents profiles of the local Nusselt number along the heater for different values of the Richardson number. An increase in Ri leads to a growth of Nu along the heater. At the same time, the Nusselt number decreases from the left side of the heater till $x \sim 0.61$ and increases for $x > 0.62$. The physical reason for such behavior is a formation of ascending thermal boundary layer over the heater, and the maximum value of the Nusselt number occurs at the beginning of the layer. A local increase in Nu near the right border of the heater is due to a stopping of the heater effect.

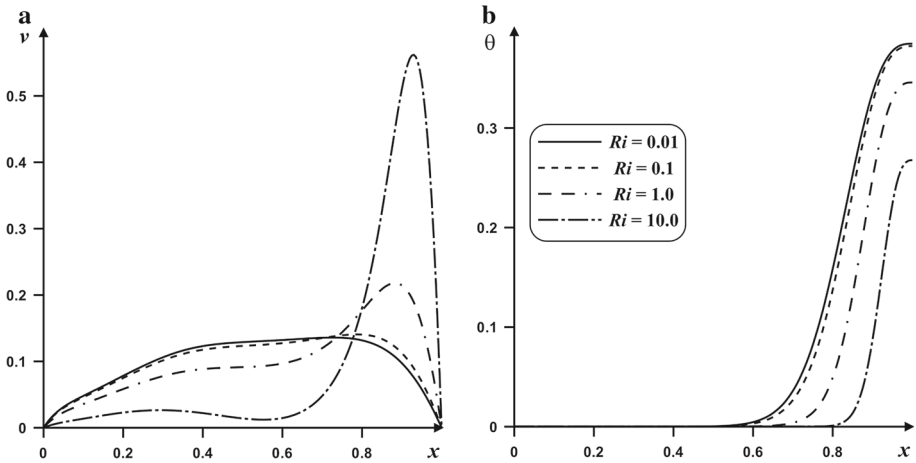
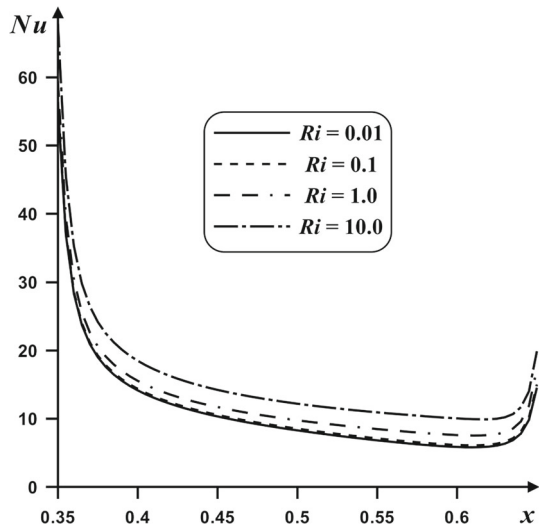


Fig. 6 Profiles of vertical velocity v (a) and temperature θ (b) at middle cross section $y = 0.5$ for case (I) at $Da = 10^{-3}$, $\delta = 0.3$ and different Richardson numbers

Fig. 7 Profiles of local Nusselt number along the heater for case (I) at $Da = 10^{-3}$, $\delta = 0.3$ and different Richardson numbers



The effect of the Darcy number on the fluid flow and heat transfer is presented in Fig. 8. Low values of Da ($Da \leq 10^{-4}$) illustrate low intensive flow where the fluid occupies the whole porous layer without recirculations inside the cavity. An increase in the Darcy number ($Da = 10^{-1}$) leads to a formation of the convective cell over the porous layer due to more essential effect of the buoyancy force when the permeability of the medium is significant and close to the clear fluid. The temperature field also reflects a formation of the thermal plume near the right vertical adiabatic wall.

More detailed description of the velocity components and the temperature profiles is presented in Figs. 9 and 10 for the middle cross sections $x = 0.5$ and $y = 0.5$ for the case of horizontal and vertical velocity components. The temperature profiles with Da are similar to the effect of the Richardson number (Figs. 5, 6). As for the velocity components, it should be noted that the typical velocity behavior close to the solid walls inside the porous layer for

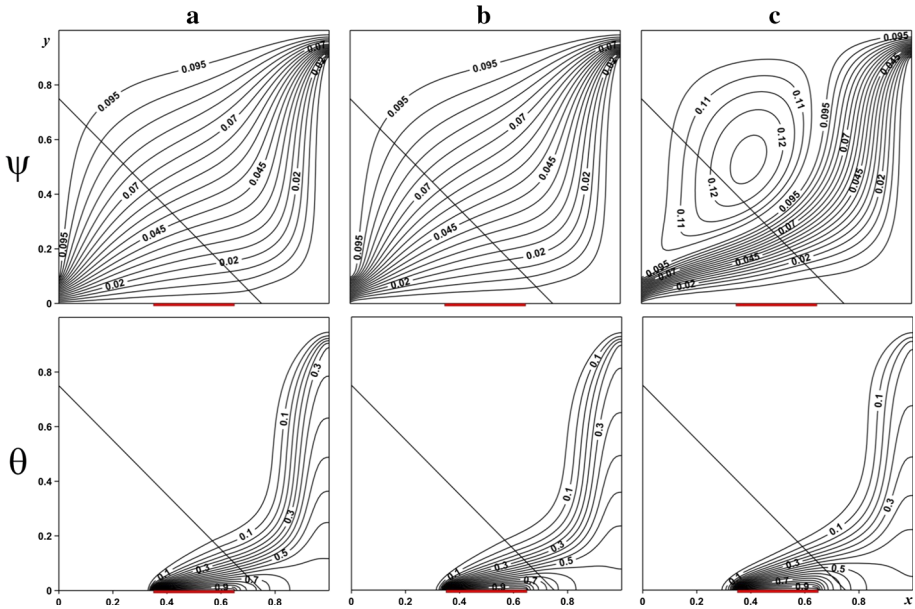


Fig. 8 Streamlines ψ and isotherms θ for case (I) at $Ri = 1.0$, $\delta = 0.3$: $Da = 10^{-7}$ (a), $Da = 10^{-4}$ (b), $Da = 10^{-1}$ (c)

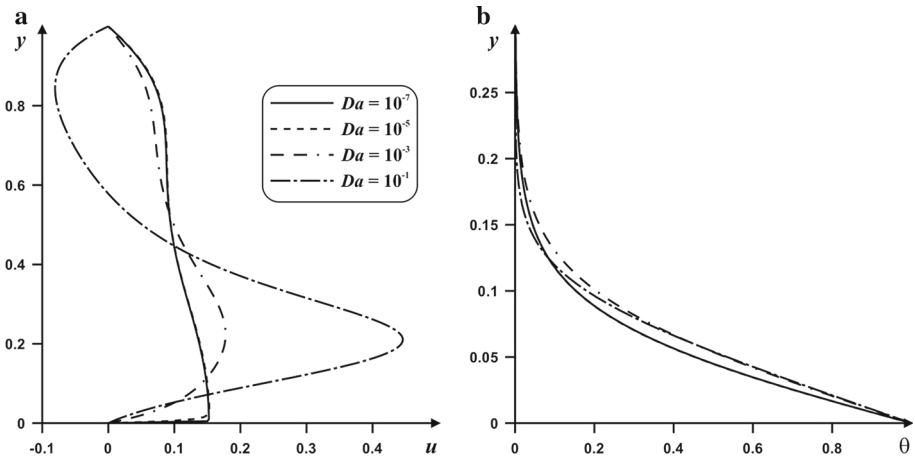


Fig. 9 Profiles of horizontal velocity u (a) and temperature θ (b) at middle cross section $x = 0.5$ for case (I) at $Ri = 1.0$, $\delta = 0.3$ and different Darcy numbers

low Darcy numbers ($Da \leq 10^{-5}$) is with essential velocity gradient (Sheremet and Trifonova 2013, 2014). An increase in the permeability of the medium leads to an essential growth of the velocity in the bottom part and a formation of a reverse flow near the upper part.

Variations of the average Nusselt number at the heater with Da and Ri are presented in Fig. 11. As has been mentioned above, an increase in Ri leads to a heat transfer enhancement. The maximum Nusselt number is recorded at the lower value of Darcy number ($Da = 10^{-7}$), and this can be attributed to the large drag exerted by the lower permeable porous medium

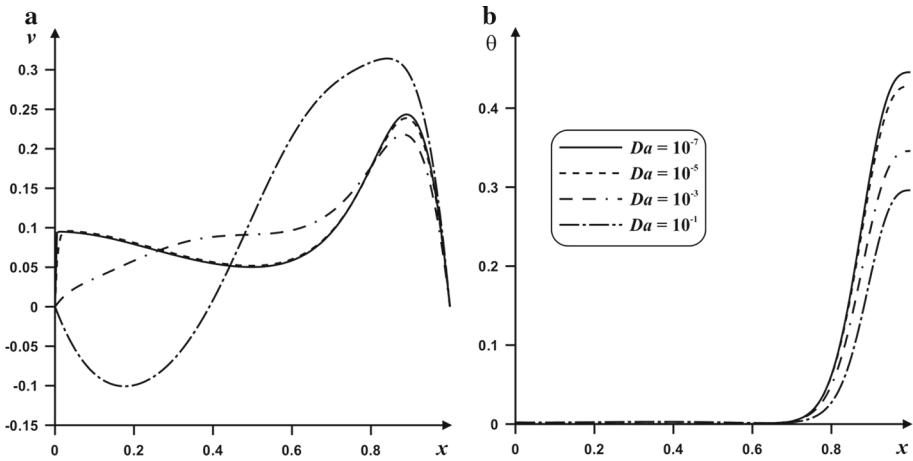
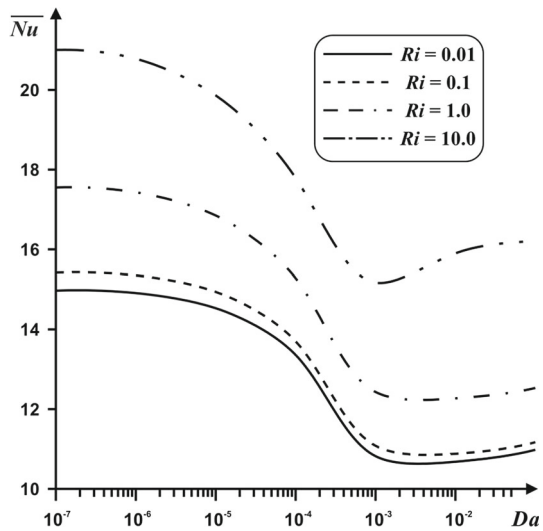


Fig. 10 Profiles of vertical velocity v (a) and temperature θ (b) at middle cross section $y = 0.5$ for case (I) at $Ri = 1.0$, $\delta = 0.3$ and different Darcy numbers

Fig. 11 Variations of average Nusselt number at the heater for case (I) for $\delta = 0.3$ and different values of Richardson and Darcy numbers



which in turn reduce the penetration of water entering the cavity. As such, the diffusion phenomenon is less significant compared with the convective heat transfer. A growth of the Darcy number until a critical value of 10^{-3} illustrates a reduction in heat transfer rate. This is because the reduction in the drag force stimulates the conductive heat transfer, while for $Da > 10^{-3}$ one can find a rise of the average Nusselt number due to a more significant influence of the buoyancy force for the medium with a high permeability. At the same time, it should be noted that it is a partially porous cavity and we have to take into account the momentum and energy interactions between porous layer and clear fluid at interface, while the heater is located near this boundary. An increase in porous layer thickness can lead to a formation of classical behavior when a growth of Darcy number leads to the heat transfer enhancement. Therefore, the main reason for such behavior is a proximity to the porous–fluid

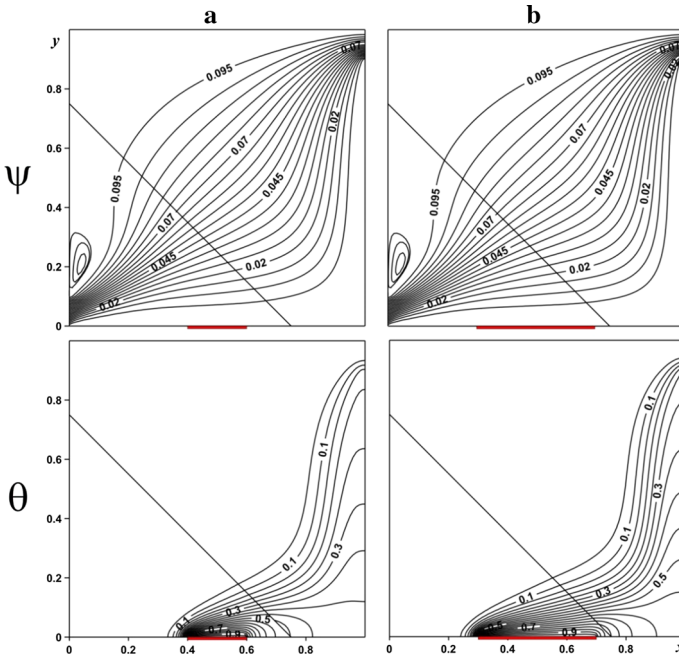


Fig. 12 Streamlines ψ and isotherms θ for case (I) at $Ri = 1.0, Da = 10^{-3}$: $\delta = 0.2$ (a), $\delta = 0.4$ (b)

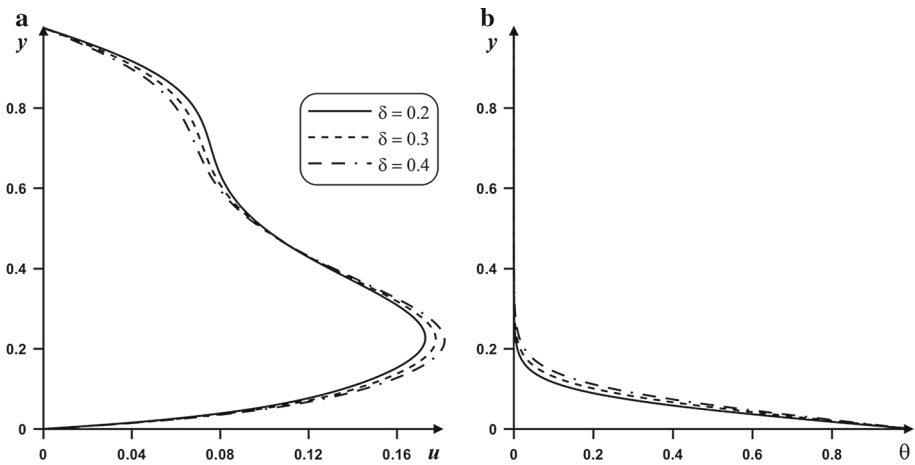


Fig. 13 Profiles of horizontal velocity u (a) and temperature θ (b) at middle cross section $x = 0.5$ for case (I) at $Ri = 1.0, Da = 10^{-3}$ and different values of heater length

interface combined with above mentioned physical features. It is worth noting that a high rate of the average Nusselt number growth is at high values of the Richardson number.

Figures 12, 13 and 14 show the effect of the heater length on the streamlines, isotherms and the profiles of the temperature and velocity components. As expected, an increase in δ leads to more essential heating of the cavity bottom part, and as a result, the average temperature inside the cavity increases. A growth of the horizontal velocity in the bottom

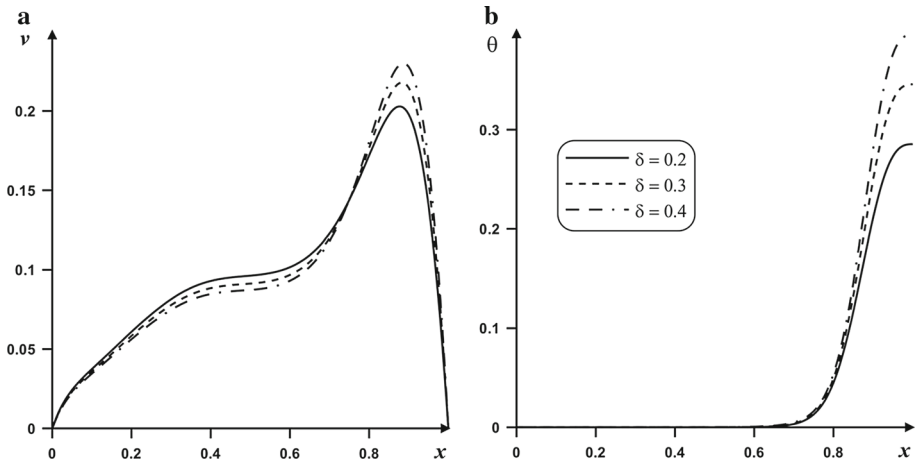
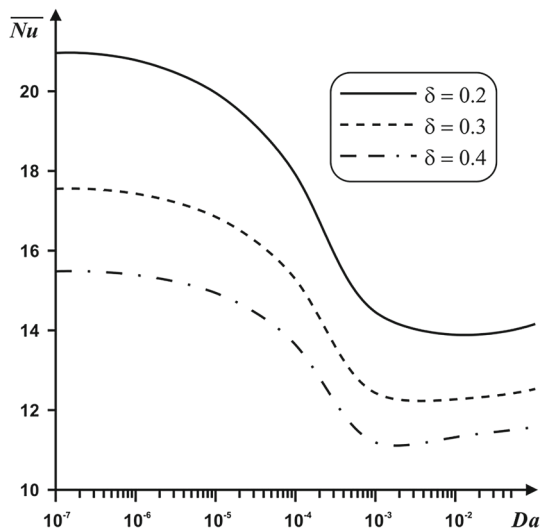


Fig. 14 Profiles of vertical velocity v (a) and temperature θ (b) at middle cross section $y = 0.5$ for case (I) at $Ri = 1.0$, $Da = 10^{-3}$ and different values of heater length

Fig. 15 Variations of average Nusselt number at the heater for case (I) at $Ri = 1.0$ and different values of heater length and Darcy number



part due to a continuing effect of the buoyancy force is presented in Fig. 13a. At the same time, a reduction of u in the upper part (Fig. 13a) and v in the left part (Fig. 14a) can be explained by an interaction between the buoyancy force and the inertia force. A growth of temperature with the heater length is presented in Figs. 13b and 14b. It is worth noting that at the right vertical wall ($y = 0.5$), an increase in the heater length from 0.2 till 0.4 leads to a growth of the temperature from 0.29 till 0.40 and the dimensionless vertical velocity component rises from 0.20 till 0.23.

Figure 15 presents the variations of the average Nusselt number at the heater with the heater length and the Darcy number. An increase in the heater length leads to a reduction in the heat transfer rate, and a more essential decrease in \overline{Nu} occurs for a rise of the heater length from 0.2 till 0.3.

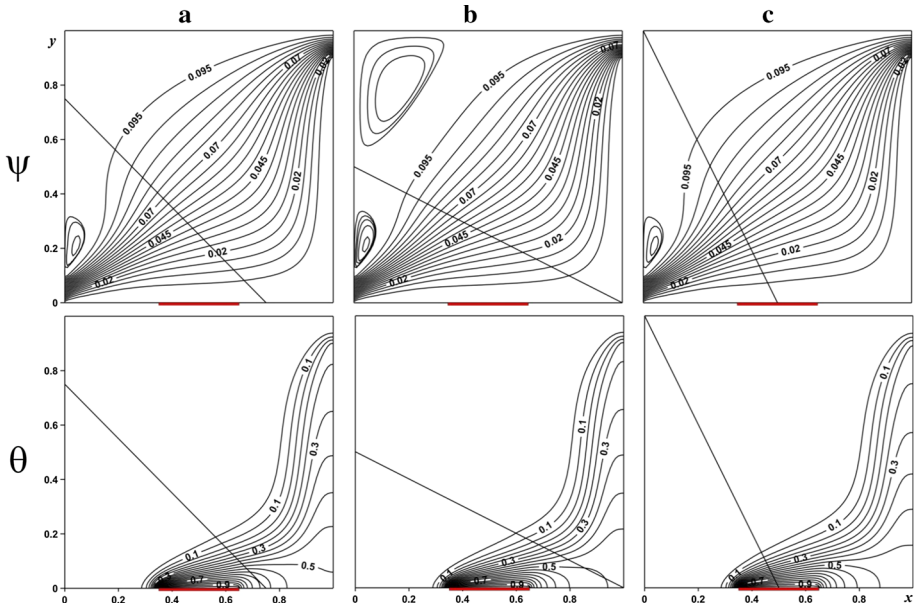


Fig. 16 Streamlines ψ and isotherms θ at $Ri = 1.0$, $Da = 10^{-3}$, $\delta = 0.3$: case (I) (a), case (II) (b), case (III) (c)

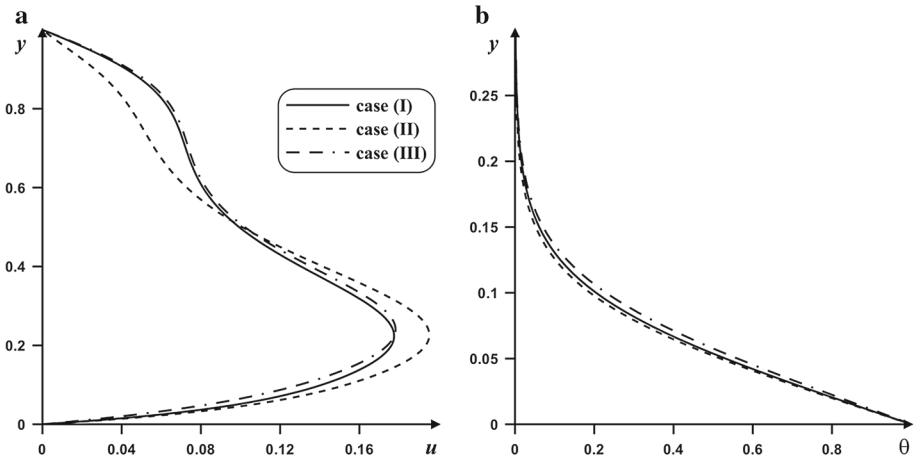


Fig. 17 Profiles of horizontal velocity u (a) and temperature θ (b) at middle cross section $x = 0.5$ for $Ri = 1.0$, $Da = 10^{-3}$, $\delta = 0.3$ and different cases

The effect of different porous layer positions on the streamlines, isotherms and the profiles of velocity and temperature is presented in Figs. 16, 17 and 18. The main feature is that an increase in the distance between the top wall and the porous layer leads to a formation of a convective cell inside the cavity (Fig. 15b), while the other parameters concerning the fluid flow and heat transfer patterns are the same. The abovementioned feature illustrates an increase in the horizontal velocity at the bottom part (Fig. 17a) due to a small deformation of the main incoming flow, and as a result, one can find a weak velocity reduction in the upper

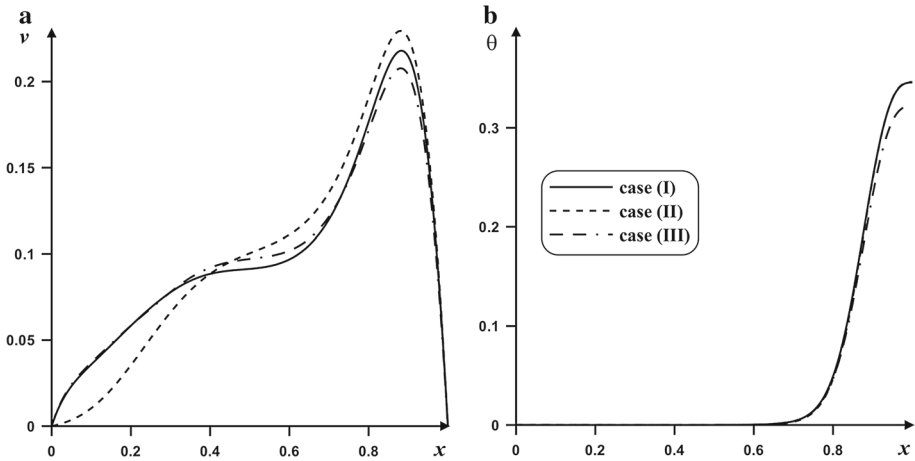
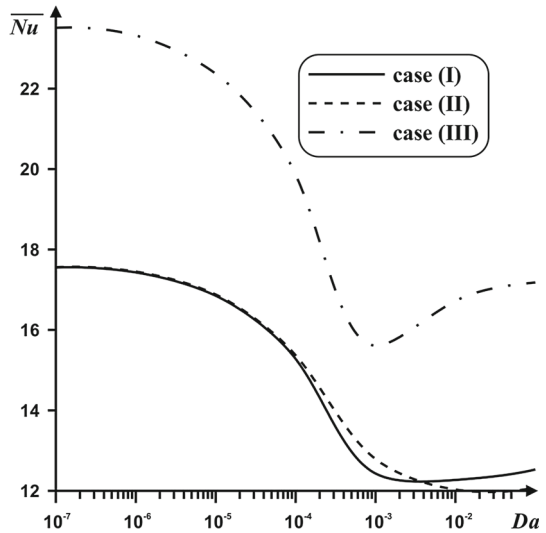


Fig. 18 Profiles of vertical velocity v (a) and temperature θ (b) at middle cross section $y = 0.5$ for $Ri = 1.0$, $Da = 10^{-3}$, $\delta = 0.3$ and different cases

Fig. 19 Variations of average Nusselt number at the heater for $Ri = 1.0$, $\delta = 0.3$, different cases and Darcy numbers



part. Such intensification of the fluid flow illustrates an increase in the temperature in the central part of the cavity.

Figure 19 demonstrates the heat transfer enhancement for the case (III) when the heater is half-covered by the porous layer. As a result, a lack of the solid matrix of the porous medium leads to an essential intensification of the heat transfer.

5 Conclusion

A numerical analysis of the mixed convection in an open cavity partially filled with a porous medium in the presence of a local heater has been carried out in a wide range of the Richard-

son and Darcy numbers, as well as the heater length and location of the porous layer. The governing equations formulated in the dimensionless stream function, vorticity and temperature have been solved by the finite difference method using the Brinkmann–extended Darcy model for the porous layer. The obtained results presented for the distributions of streamlines, isotherms and the profiles of velocity and temperature as well as the local and average Nusselt number profiles reveal the following:

1. An increase in the Richardson number leads to an intensification of the fluid flow and heat transfer. High values of Ri illustrate a formation of additional recirculation inside the cavity. At the same time, the dimensionless temperature decreases in the right part of the cavity.
2. A growth of the Darcy number reflects a reduction in the heat transfer rate for $Da < 10^{-3}$, while the following increase for $Da > 10^{-3}$ characterizes a heat transfer enhancement. It should be noted that high values of the Darcy number lead to a formation of a convective cell inside the cavity due to more essential effect of the buoyancy force.
3. A rise of the heater length illustrates the diminution of the heat transfer rate with an intensification of the flow and increase in the average temperature for a long heater.
4. An increase in the distance between the top wall and the porous layer leads to a formation of a convective cell inside the cavity, while the heat transfer enhancement occurs for the case (III) when the heater is half-covered by the porous layer.

Acknowledgements This work of Nikita S. Gibanov was conducted as a government task of the Ministry of Education and Science of the Russian Federation (Project Number 13.9724.2017/8.9). The authors also wish to express their thank to the very competent reviewers for the valuable comments and suggestions.

References

- Angirasa, D.: Mixed convection in a vented enclosure with an isothermal vertical surface. *Fluid Dyn. Res.* **26**, 219–233 (2000)
- Anil Lal, S., Reji, C.: Numerical prediction of natural convection in vented cavities using restricted domain approach. *Int. J. Heat Mass Transf.* **52**, 724–734 (2009)
- Arpino, F., Cortellessa, G., Mauro, A.: Transient thermal analysis of natural convection in porous and partially porous cavities. *Numer. Heat Transf. A* **67**, 605–631 (2015)
- Bagchi, A., Kulacki, F.A.: Experimental study of natural convection in fluid-superposed porous layers heated locally from below. *Int. J. Heat Mass Transf.* **55**, 1149–1153 (2012)
- Bahlaoui, A., Raji, A., Hasnaoui, M., Naïmi, M.: Mixed convection heat transfer enhancement in a vented cavity filled with a nanofluid. *J. Appl. Fluid Mech.* **9**, 593–604 (2016)
- Beavers, G.S., Joseph, D.D.: boundary conditions at a naturally permeable wall. *J. Fluid Mech.* **30**, 197–207 (1967)
- Beckermann, C., Ramadhyani, S., Viskanta, R.: Natural convection flow and heat transfer between a fluid layer and a porous layer inside a rectangular enclosure. *ASME J. Heat Transf.* **109**, 363–370 (1987)
- Behzadi, T., Shirvan, K.M., Mirzahalalari, S., Sheikhrabat, A.A.: Numerical simulation on effect of porous medium on fixed convection heat transfer in a ventilated square cavity. *Procedia Eng.* **127**, 221–228 (2015)
- Besbes, S., Mhiri, H., El Golli, S., Le Palec, G., Bournot, P.: Numerical study of a heated cavity insulated by a horizontal laminar jet. *Energy Convers. Manag.* **42**, 1417–1435 (2001)
- Bhardwaj, S., Dalal, A., Pati, S.: Influence of wavy wall and non-uniform heating on natural convection heat transfer and entropy generation inside porous complex enclosure. *Energy* **79**, 467–481 (2015)
- Biserni, C., Rocha, L.A.O., Stanescu, G., Lorenzini, E.: Constructural H-shaped cavities according to Bejan's theory. *Int. J. Heat Mass Transf.* **50**, 2132–2138 (2007)
- Boulard, T., Kittas, C., Roy, J.C., Wang, S.: Convective and ventilation transfers in greenhouses, part 2: determination of the distributed greenhouse climate. *Biosyst. Eng.* **83**(2), 129–147 (2002)
- Chamkha, A.J., Ismael, M.A.: Natural convection in differentially heated partially porous layered cavities filled with a nanofluid. *Numer. Heat Transf. A* **65**, 1089–1113 (2014)

- Chen, F., Chen, C.F.: Convection in superposed fluid and porous layers. *J. Fluid Mech.* **234**, 97–119 (1992)
- Chen, K.S., Humphery, J.A.C., Sherman, F.S.: Experimental investigation of thermally driven flow in open cavities of rectangular cross-section. *Philos. Trans. R. Soc. Lond. A* **316**, 57–84 (1985)
- Choi, S.U.S., Eastman, J.A.: Enhancing thermal conductivity of fluids with nanoparticles. In: ASME International Mechanical Engineering Congress and Exposition, San Francisco (1995)
- Desai, C., Vafai, K.: Three-dimensional buoyancy-induced flow and heat transfer around the wheel outboard of an aircraft. *Int. J. Heat Fluid Flow* **13**, 50–64 (1992)
- Elsayed, M.M., Chakroun, W.: Effects of aperture geometry on heat transfer in tilted partially open cavities. *J. Heat Transf.* **121**, 819–827 (1999)
- Ghalambaz, M., Moattar, F., Karbassi, A., Sheremet, M.A., Pop, I.: Triple-diffusive mixed convection in a porous open cavity. *Transp. Porous Media* **116**, 473–491 (2017)
- Gobin, D., Goyeau, B., Neculae, A.: Convective heat and solute transfer in partially porous cavities. *Int. J. Heat Mass Transf.* **48**, 1898–1908 (2005)
- Hirata, S.C., Goyeau, B., Gobin, D., Chandesris, M., Jamet, D.: Stability of natural convection in superposed fluid and porous layers: equivalence of the one-and two-domain approaches. *Int. J. Heat Mass Transf.* **52**, 533–536 (2009)
- Ingham, D.B., Pop, I. (eds.): *Transport Phenomena in Porous Media III*. Elsevier, Oxford (2005)
- Ismail, M.A., Chamkha, A.J.: Conjugate natural convection in a differentially heated composite enclosure filled with a nanofluid. *J. Porous Media* **18**, 699–716 (2015)
- Khanafar, K., Vafai, K.: Buoyancy-driven flows and heat transfer in open-ended enclosures: elimination of the extended boundaries. *Int. J. Heat Mass Transf.* **43**, 4087–4100 (2000)
- Khanafar, K., Vafai, K., Lightston, M.: Mixed convection heat transfer in two-dimensional open-ended enclosures. *Int. J. Heat Mass Transf.* **45**, 5171–5190 (2002)
- Khanafar, K., Vafai, K.: Effective boundary conditions for buoyancy-driven flows and heat transfer in fully open ended two-dimensional enclosures. *Int. J. Heat Mass Transf.* **45**, 2527–2538 (2002)
- Kim, J.H., Ochoa-Tapia, J.A., Whitaker, S.: Diffusion in anisotropic porous media. *Transp. Porous Media* **2**, 327–356 (1987)
- Kim, S.G., Choi, C.Y.: Convective heat transfer in porous and overlying fluid layers heated from below. *Int. J. Heat Mass Transf.* **39**, 319–329 (1996)
- Kuznetsov, G.V., Sheremet, M.A.: Numerical simulation of convective heat transfer modes in a rectangular area with a heat source and conducting walls. *J. Heat Transf.* **132**, 1–9 (2010)
- Lauriat, G., Prasad, V.: Non-Darcian effects on natural convection in a vertical porous enclosure. *Int. J. Heat Mass Transf.* **32**, 2135–2148 (1989)
- Lopez, J.J., Tapia, J.A.: A study of buoyancy driven flow in a confined fluid overlying porous layer. *Int. J. Heat Mass Transf.* **44**, 4725–4736 (2001)
- Mahmoudi, A.H., Shahi, M., Talebi, F.: Effect of inlet and outlet location on the mixed convective cooling inside the ventilated cavity subjected to an external nanofluid. *Int. Commun. Heat Mass Transf.* **37**, 1158–1173 (2010)
- Mahmud, S., Pop, I.: Mixed convection in a square vented enclosure filled with a porous medium. *Int. J. Heat Mass Transf.* **49**, 2190–2206 (2006)
- Mezrhab, A., Amraqui, S., Abid, C.: Modeling of combined surface radiation and natural convection in a vented “T” form cavity. *Int. J. Heat Fluid Flow* **31**, 83–92 (2010)
- Mhiri, H., El Golli, S., Berthon, A., Le Palec, G., Bournot, P.: Numerical study of the thermal and aerodynamic insulation of a cavity with a vertical downstream air jet. *Int. Commun. Heat Mass Transf.* **25**, 919–928 (1998)
- Nasrin, R., Alim, M.A., Chamkha, A.J.: Numerical simulation of non-Darcy forced convection through a channel with non-uniform heat flux in an open cavity using nanofluid. *Numer. Heat Transf. A* **64**, 820–840 (2013)
- Neale, G., Nader, W.: Practical significance of Brinkman’s extension of Darcy’s law: coupled parallel flows within a channel and a bounding porous medium. *Can. J. Chem. Eng.* **52**, 475–478 (1974)
- Nield, D.A., Bejan, A.: *Convection in Porous Media*, 5th edn. Springer, New York (2017)
- Pardeshi, I.A.: Flow and Heat Transfer in an L-shaped Cooling Passage with Ribs and Pin Fins for the Trailing Edge of a Gas-Turbine Vane and Blade. *Open Access Theses*. Paper 87 (2013)
- Raji, A., Hasnaoui, M., Bahlaoui, A.: Numerical study of natural convection dominated heat transfer in a ventilated cavity: case of forced flow playing simultaneous assisting and opposing roles. *Int. J. Heat Fluid Flow* **29**, 1174–1181 (2008)
- Shahi, M., Mahmoudi, A.H., Talebi, F.: Numerical study of mixed convective cooling in a square cavity ventilated and partially heated from the below utilizing nanofluid. *Int. Commun. Heat Mass Transf.* **37**, 201–213 (2010)

- Shenoy, A., Sheremet, M.A., Pop, I.: Convective Flow and Heat Transfer from Wavy Surfaces: Viscous Fluids, Porous Media and Nanofluids. CRC Press, Boca Raton (2016)
- Sheremet, M.A., Pop, I., Ishak, A.: Double-diffusive mixed convection in a porous open cavity filled with a nanofluid using Buongiorno's model. *Transp. Porous Media* **109**, 131–145 (2015)
- Sheremet, M.A., Trifonova, T.A.: Unsteady conjugate natural convection in a vertical cylinder partially filled with a porous medium. *Numer. Heat Transf. A* **64**, 994–1015 (2013)
- Sheremet, M.A., Trifonova, T.A.: Unsteady conjugate natural convection in a vertical cylinder containing a horizontal porous layer: Darcy model and Brinkman-extended Darcy model. *Transp. Porous Media*. **101**, 437–463 (2014)
- Showole, R.A., Tarasuk, J.D.: Experimental and numerical studies of natural convection with flow separation in upward-facing inclined open cavities. *J. Heat Transf.* **115**, 592–605 (1993)
- Singh, A.K., Thorpe, G.R.: Natural convection in a confined fluid overlying a porous layer-A comparison study of different models. *Indian J. Pure Appl. Math.* **26**, 81–95 (1995)
- Tiwari, R.K., Das, M.K.: Heat transfer augmentation in a two-sided lid-driven differentially heated square cavity utilizing nanofluids. *Int. J. Heat Mass Transf.* **50**, 2002–2018 (2007)
- Vafai, K., Etefagh, J.: The effects of sharp corners on buoyancy-driven flows with particular emphasis on outer boundaries. *Int. J. Heat Mass Transf.* **33**, 2311–2328 (1990)
- Vafai, K., Etefagh, J.: Thermal and fluid flow instabilities in buoyancy-driven flows in open-ended cavities. *Int. J. Heat Mass Transf.* **33**, 2329–2344 (1990)
- Vafai, K. (ed.): *Handbook of Porous Media*, 3rd edn. CRC Press, Boca Raton (2015)
- Xu, H., Xiao, R., Karimi, F., Yang, M., Zhang, Y.: Numerical study of double diffusive mixed convection around a heated cylinder in an enclosure. *Int. J. Therm. Sci.* **78**, 169–181 (2014)
- Zhao, P., Chen, C.F.: Stability analysis of double-diffusive convection in superposed fluid and porous layers using a one-equation model. *Int. J. Heat Mass Transf.* **44**, 4625–4633 (2001)